Environmental Pollution 239 (2018) 392–398

Contents lists available at ScienceDirect

Environmental Pollution

journal homepage: www.elsevier.com/locate/envpol

Nitrogen isotope variations of ammonium across rain events: Implications for different scavenging between ammonia and particulate ammonium☆

Xu-Dong Zheng [a], Xue-Yan Liu [a, b, *], Wei Song [a], Xin-Chao Sun [a], Cong-Qiang Liu [a, b]

[a] Institute of Surface-Earth System Science, Tianjin University, Tianjin, 300072, China
[b] State Key Laboratory of Environmental Geochemistry, Institute of Geochemistry, Chinese Academy of Sciences, Guiyang, 550002, China

ARTICLE INFO

Article history:
Received 10 November 2017
Received in revised form
5 March 2018
Accepted 3 April 2018
Available online 17 April 2018

Keywords:
Stable isotope
Ammonium
Scavenging
Precipitation
$PM_{2.5}$
TSP

ABSTRACT

Enhanced ammonia (NH_3) emissions and deposition caused negative effects on air quality and ecosystems. Precipitation is an efficient pathway to remove NH_3 and particulate ammonium (p-NH_4^+) from the atmosphere into ecosystems. However, precipitation scavenging of p-NH_4^+ in chemical transport models has often considered fine p-NH_4^+, with inadequate constraints on NH_3 and coarse p-NH_4^+. Based on distinct $\delta^{15}N$ values between NH_3 and NH_4^+ in $PM_{2.5}$ (particulate matters with aerodynamic diameters ≤ 2.5 μm) or TSP (total suspended particulates), this paper interpreted intra-event variations of precipitation NH_4^+ concentrations and $\delta^{15}N$ values ($\delta^{15}N$-NH_4^+ values) at Guiyang (Xiao et al., 2015). Generally decreased NH_4^+ concentrations across rain events reflected decreasing scavenging of NH_3 and p-NH_4^+. Using a Bayesian isotope mixing model, we found that differing contributions between ^{15}N-depleted NH_3 and ^{15}N-enriched p-NH_4^+ were responsible for the three-stage variations of intra-event $\delta^{15}N$-NH_4^+ values. The decreases of $\delta^{15}N$-NH_4^+ values across the first and third stages indicated more decreases in scavenging p-NH_4^+ than NH_3, while the increases of $\delta^{15}N$-NH_4^+ values across the second stage were resulted primarily from more increases in scavenging p-NH_4^+ (particularly fine p-NH_4^+) than NH_3. These results stressed influences of differing scavenging between NH_3 and p-NH_4^+ on precipitation $\delta^{15}N$-NH_4^+ values, which should be considered in modeling precipitation scavenging of atmospheric p-NH_4^+.

1. Introduction

Ammonium (NH_4^+) is the dominant form of inorganic nitrogen (N) deposition from the atmosphere to most terrestrial ecosystems of the world (Galloway et al., 2008; Liu et al., 2013), mainly originating from combustion sources (e.g. fossil fuel consumption and biomass burning) and volatilized sources (e.g. fertilizer application and wastes) (Sutton et al., 2000; Huang et al., 2012; Kang et al., 2016). For example, increased NH_3 emissions in China were primarily derived from livestock wastes and synthetic fertilizer applications, which accounted for about 49% and 37% of annual NH_3 emissions on average from 1980 to 2012 (Kang et al., 2016). These emissions enhanced the NH_3 and NH_4^+ deposition over China (Liu et al., 2013), which has caused negative effects on air quality and ecosystems.

Precipitation is an efficient way to remove NH_3 and p-NH_4^+ from the atmosphere (Seinfeld and Pandis, 2006; Andronache, 2003; Kajino and Aikawa, 2015), generally accounting for over 72% of NH_4^+ deposition at different types of land use across China (Xu et al., 2015). Precipitation scavenging mechanisms of particulates are critical for parameterizing wet scavenging coefficients (WSCs, Xu et al., 2017) in chemical transport models (Wang et al., 2014; Xu et al., 2017). Since 1990s, scavenging coefficients have become quite important parameters in chemical transport models to characterize precipitation processes (Okita et al., 1996; Zhang et al., 2013). However, there have long been substantial uncertainties (such as size-specific scavenging coefficients and vertical variations of aerosols) in theoretical parameterizations of WSCs due to the complex physical and chemical processes in the atmosphere (Zhang et al., 2013; Sun et al., 2015).

There are two main scavenging processes of precipitation: rainout (in-cloud scavenging) and washout (below-cloud

☆ This paper has been recommended for acceptance by B. Nowack.
* Corresponding author. Institute of Surface-Earth System Science, Tianjin University, Tianjin, 300072, China.
E-mail address: liuxueyan@tju.edu.cn (X.-Y. Liu).

https://doi.org/10.1016/j.envpol.2018.04.015
0269-7491/

scavenging) (Andronache, 2003). The rainout and washout mechanisms of particulates include the activation of cloud condensation nuclei in supersaturation conditions and the collection of aerosols by falling hydrometeors, respectively (Andronache, 2003; Aikawa and Hiraki, 2009). For rainout, individual cloud droplets initially start their lives as cloud condensation nuclei. The critical supersaturation and the particulate diameters (particularly around one hundred nanometers) are the key factors of cloud condensation nuclei concentrations (Köhler, 1936; Dusek et al., 2006). The washout dominates the removal of atmospheric particulates due to high p-NH_4^+ concentrations below cloud and thus is a crucial process in chemical transport models (Aikawa and Hiraki, 2009; Kajino and Aikawa, 2015; Xu et al., 2017). To reduce uncertainties of parameters in models, some field studies were conducted on the WSCs of aerosols (Okita et al., 1996; Andronache, 2004; Yamagata et al., 2009). The current below-cloud WSCs of p-NH_4^+ are based on the assumption that precipitation NH_4^+ (w-NH_4^+) mainly comes from fine particulates (with aerodynamic diameters ≤ 2.5 μm; $PM_{2.5}$) (Kajino and Aikawa, 2015; Xu et al., 2017). However, this assumption remains uncertain due to inadequate consideration on NH_3 and coarse p-NH_4^+. During the precipitation, it is difficult to measure the real-time and vertical variations of atmospheric NH_3 and p-NH_4^+ concentrations (Asman et al., 1998). Both p-NH_4^+, especially in coarse particulates, and NH_3 concentrations decreased greatly with the altitude (Georgii and Muller, 1973; Zhang et al., 2009; Li et al., 2015), approaching zero over cloud base heights (e.g., 1687 m on average; Zhang et al., 2009; Xu et al., 2017). For p-NH_4^+, the scavenging coefficients of coarse particulates (with diameters >2.5 μm) are higher than those of $PM_{2.5}$ because of gentler Brownian motion and smaller inertia of fine ones (Greenfield, 1957; Andronache, 2003). Therefore, low below-cloud concentrations of coarse p-NH_4^+ relative to fine p-NH_4^+ do not necessarily represent a negligible contribution to w-NH_4^+ due to its higher scavenging coefficients (Greenfield, 1957; Andronache, 2003; Li et al., 2014). For NH_3, the Henry constant for solution in pure water is about 6.0×10^{-1} mol m^{-3} Pa^{-1} (Sander, 2015). Theoretical studies indicated that in addition to NH_3, fine p-NH_4^+ and coarse p-NH_4^+ substantially contributed to w-NH_4^+ (Behera et al., 2013; Li et al., 2014). A study at Canadian rural locations estimated high NH_3 scavenging contributions (ca. 30%) to w-NH_4^+ (Cheng and Zhang, 2017). However, based on the precipitation NH_4^+ concentrations (expressed as [NH_4^+]), it is difficult to differentiate the relative importance among NH_3, fine p-NH_4^+ and coarse p-NH_4^+ for precipitation scavenging, which is very important to estimate below-cloud WSCs of p-NH_4^+ (Yamagata et al., 2009; Xu et al., 2017).

Natural N isotopes (expressed as $\delta^{15}N$ values) of w-NH_4^+ are important parameters in recording sources and precipitation scavenging processes of atmospheric NH_3 and p-NH_4^+ (Moore, 1977; Freyer, 1978; Heaton, 1987; Altieri et al., 2014). Since 1950s, $\delta^{15}N$ values of precipitation NH_4^+ ($\delta^{15}N$-NH_4^+ values) have been applied for tracing major sources of atmospheric NH_3 (Hoering, 1956; Leng et al., 2017; Liu et al., 2017), mostly based on direct $\delta^{15}N$ comparisons between NH_4^+ in daily- or event-based rainwater and NH_3 from emission sources (e.g. Felix et al., 2013). There is a lack of knowledge on the relative importance of NH_3, fine p-NH_4^+, and coarse p-NH_4^+ to w-NH_4^+, which is important for better interpreting precipitation $\delta^{15}N$-NH_4^+ values and variations. Due to the development of $\delta^{15}N$ analytical methods (Garten, 1992; Liu et al., 2014), $\delta^{15}N$ values of NH_3 and p-NH_4^+ were characterized in different field circumstances in past decades (Fig. 1). The observed $\delta^{15}N$ values showed distinct differences among NH_3, NH_4^+ in $PM_{2.5}$ and TSP (total suspended particulates) (hereafter expressed as $PM_{2.5}$-NH_4^+ and TSP-NH_4^+, respectively) (Fig. 1). Due to the large kinetic isotope fractionations during agricultural NH_3 volatilization, the $\delta^{15}N$ values (mean ± SD values) of NH_3 (−16.7 ± 11.5‰; n = 122; Smirnoff et al., 2012; Chang et al., 2016; Felix et al., 2017; Savard et al., 2017) are significantly lower than those of $PM_{2.5}$-NH_4^+ ($\delta^{15}N_{PM2.5\text{-}NH4+}$: 6.6 ± 10.2‰; n = 184; Smirnoff et al., 2012; Proemse et al., 2012; Lin et al., 2016; Park et al., 2017) and TSP-NH_4^+ ($\delta^{15}N_{TSP\text{-}NH4+}$: 16.1 ± 6.8‰; n = 94; Yeatman et al., 2001; Kundu et al., 2010; Savard et al., 2017) ($p < 0.05$) (Fig. 1). For atmospheric NH_3, the relative contributions of different NH_3 emission sources directly determine its $\delta^{15}N$ signatures and ranges. Differently, ^{15}N enrichment in p-NH_4^+ relative to NH_3 is mainly caused by the large fractionations of equilibrium reaction between NH_3 and p-NH_4^+ (Heaton et al., 1997). The p-NH_4^+ is mostly produced by the secondary reactions of NH_3 with acids, with quite lower contributions from primary particulates. Accordingly, different NH_3 emission sources with different NO_x and SO_2 emissions (Seinfeld and Pandis, 2006; Wang et al., 2013) potentially influence the $NH_3 \leftrightarrow NH_4^+$ equilibrium and associated isotope effects thus the $\delta^{15}N$ values of corresponding p-NH_4^+. Depending on *in-situ* physical and chemical conditions, p-NH_4^+ may experience more equilibrium exchanges with NH_3 during the long-range transportation (Skinner et al., 2004, 2006; Felix et al., 2014). As fine particulates have already included in and mixed with the coarse particulates during the collection of TSP, $\delta^{15}N_{TSP\text{-}NH4+}$ values were virtually the bulk $\delta^{15}N$ values of fine and coarse p-NH_4^+. If the equilibrium isotope effects with NH_3 do not differ between TSP-NH_4^+ and $PM_{2.5}$-NH_4^+, one possible reason for higher $\delta^{15}N$ values in TSP-NH_4^+ than $PM_{2.5}$-NH_4^+ is that TSP includes more primary NH_4^+ sources (e.g., $\delta^{15}N$ = about 20 − 34‰ for primary p-NH_4^+ from livestock wastes; Savard et al., 2017) than $PM_{2.5}$ (Wang et al., 2011, 2013; Guo et al., 2014). Differently, $PM_{2.5}$-NH_4^+ is chiefly produced by the secondary reactions between ^{15}N-depleted NH_3 (Fig. 1) and acids (Seinfeld and Pandis, 2006; Wang et al., 2013).

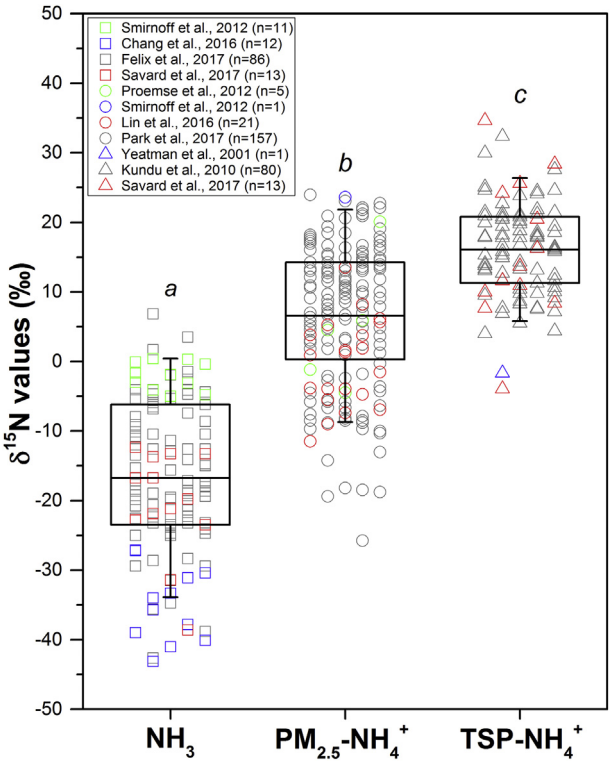

Fig. 1. $\delta^{15}N$ values of atmospheric NH_3, $PM_{2.5}$-NH_4^+, and TSP-NH_4^+. Different symbols showed scattered values. The boxes encompass the 25th − 75th percentiles, the line in each box marks the mean value, and whiskers are SD values. Different letters (*a, b, c*) above the boxes mark significant differences at the level of $P < 0.05$.

Intra-event $\delta^{15}N$ variations of N ions contain critical information on scavenging mechanisms of gaseous and particulate N precursors (Heaton, 1987), but very few works have been conducted on NH_4^+. For NO_3^-, studies revealed the role of air mass back trajectories and atmospheric oxidation in regulating intra-event $\delta^{15}N$ variations of NO_3^- (Buda and DeWalle, 2009; Felix et al., 2015). Heaton (1987) stressed the importance of selective washout of N bearing compounds in controlling $\delta^{15}N$ variations of NO_3^- during storms. Unfortunately, no further work has been conducted to test this hypothesis. For NH_4^+, Xiao et al. (2015) interpreted the intra-event variations of NH_4^+ concentrations and $\delta^{15}N$ values based on the Rayleigh model. However, the interpretation based on the Rayleigh model has had to assume precipitation NH_4^+ pools as closed systems (Xiao et al., 2015). Moreover, the in-cloud and below-cloud p-NH_4^+ contributions to precipitation NH_4^+, and the differing scavenging of NH_3 and p-NH_4^+ have not been well considered. Based on the steady state box model, the study by Altieri et al. (2014) has stressed influences of scavenging both NH_3 and p-NH_4^+ on precipitation $\delta^{15}N$-NH_4^+ values. This study aimed to characterize $\delta^{15}N$ differences between NH_3 and p-NH_4^+ ($PM_{2.5}$-NH_4^+ or TSP-NH_4^+) and then interpret intra-event $\delta^{15}N$-NH_4^+ variations (Fig. 2b) observed at Guiyang by Xiao et al. (2015). Different scavenging between NH_3 and p-NH_4^+ (TSP-NH_4^+ or $PM_{2.5}$-NH_4^+) across rain events can improve the understanding of precipitation $\delta^{15}N$-NH_4^+ values and provide useful information for modeling precipitation scavenging of atmospheric p-NH_4^+.

2. Materials and methods

2.1. Study site and sample collection

The study site was located in the Institute of Geochemistry, Chinese Academy of Sciences (CAS) (106°43′ E, 26°34′ N), which is a typical urban site of Guiyang, southwestern China. Guiyang is one of the major cities suffering from severe acid deposition since the 1980s (Xiao et al., 2015). The annual rainfall at Guiyang (1174 mm in 2009) has a distinct seasonality, with 70% falling during the warmer months (April to September) and much less precipitation in the cooler months (October to March).

Precipitation samples were collected on the roof of a building of the State Key Laboratory of Environmental Geochemistry, CAS (Xiao et al., 2015). Briefly, rain samples were collected by using two aluminous sheets (projection area: 2.1 m × 1.7 m), which was fixed 1.5 m above the roof of a building by aluminous-alloy bracket. Before sampling, the aluminous sheets were cleaned with Milli-Q water and dried. Between rain events, the collection device was covered with a large clean polyethylene sheet in order to avoid the dry deposition and other pollutants. When each rain event began, the polyethylene sheet was removed, then rainwater from the aluminous sheets was collected sequentially by acid-cleaned plastic bottles. The time lengths of sample collections were determined roughly by the demand of rain water amount for chemical analyses, depending on corresponding rain intensities. In this study, rain

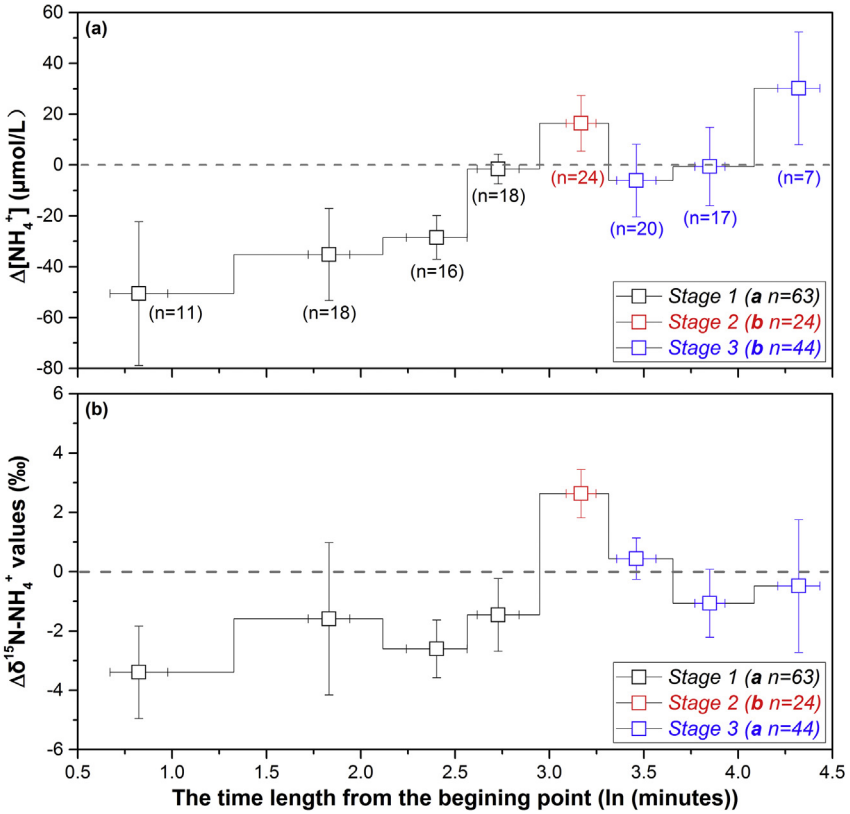

Fig. 2. The patterns of precipitation NH_4^+ concentrations (a) and $\delta^{15}N$-NH_4^+ (b) variations along the time course of rain events at Guiyang, SW China. The time course was shown by the time lengths (in Ln, because of very variable time lengths and sampling intervals among different events) from each sampling point to the beginning point of each event. Precipitation $\delta^{15}N$-NH_4^+ variations were depicted by the differences of $\delta^{15}N$-NH_4^+ values between two adjacent rain samples along each event ($\Delta\delta^{15}N$-NH_4^+: $\delta^{15}N$-NH_4^+ values of the later sample minus that of the former one). The $\Delta\delta^{15}N$-NH_4^+ values of positive, zero and negative values indicated increases, no difference and decreases. The squares and bars (both X and Y) showed mean values and SE values, respectively. Different letters (*a, b, c*) in the legend mark significant differences at the level of $P < 0.05$. As events with too short time lengths or with too long intervals between adjacent collections could not be integrated together, 12 out of 20 rain events (Xiao et al., 2015) were used to show the integrated pattern in this study. Details of rain events are given in Fig. S1.

water samples of 12 events (from 31st-Oct, 2008 to 29th-Sept, 2009) were collected (Xiao et al., 2015). Upon collection, precipitation samples were filtered using a 0.45 μm acetate membrane filters. The filtered samples were poisoned by adding $HgCl_2$ and frozen to prevent microbial conversion before concentration and nitrogen isotope analyses of NH_4^+.

2.2. Chemical analyses

The $[NH_4^+]$ in rain samples were determined colorimetrically (detailed in Xiao et al., 2015). For $\delta^{15}N$ analysis, NH_4^+ in rain samples was separated, purified, and converted to $(NH_4)_2SO_4$ or NH_4HSO_4 salts using the diffusion method (detailed in Xiao et al., 2015). Similar to Sebilo et al. (2004), about 50 μg-N of NH_4^+ salts were weighed into small tin cups (φ3.5 × 5) and then analyzed for N isotopes ($^{15}N/^{14}N$) by an elemental analyzer combustion continuous flow isotope ratio mass spectroscopy (EA-C-CF-IRMS, EAIsoPrime 100, Euro3000, GV instruments, United Kingdom). Milli-Q water in empty sampling bottles was measured by the same method as precipitation samples for blank calibrations. One international standard (IAEA-N-2; $(NH_4)_2SO_4$, $\delta^{15}N = 20.3‰$) and two laboratory standards (KNO_3, $\delta^{15}N = 21.17 \pm 0.34‰$ and $-1.98 \pm 0.16‰$, respectively) were measured with the samples for isotopic calibrations. The analytical precision was better than 0.1‰ (Xiao et al., 2015). The natural abundance of ^{15}N ($\delta^{15}N$) was expressed in parts per mil by multiplying them by 1000:

$$\delta^{15}N = \left(R_{sample} / R_{standard}\right) - 1, \quad (1)$$

where R_{sample} and $R_{standard}$ are $^{15}N/^{14}N$ in samples and the standard (atmospheric N_2), respectively.

2.3. Statistical analyses

Statistical analyses were conducted by SPSS 12.0 software packages for Windows (SPSS science, Chicago, USA). One-way ANOVA (Duncan and LSD (Least Significant Difference) methods) was performed for examining statistically significant differences at the level of $P < 0.05$.

3. Results

3.1. Precipitation $[NH_4^+]$ along the time course of rain events

The durations of rain events ranged from 12 minutes to 102 minutes, and the time intervals between adjacent sample collections varied from less than 1 minute to 22 minutes (Fig. S1). The $[NH_4^+]$ varied between 29.1 μmol/L and 675.2 μmol/L for rain samples of all events, showing distinct intra-event fluctuations (with magnitude of 0 − 307.4 μmol/L between adjacent sample collections) (Fig. S1a). Generally, a decreasing pattern existed for the $[NH_4^+]$ along the time course of almost all events, but the variations of precipitation $[NH_4^+]$ actually exhibited three stages of decreasing, increasing, and decreasing across the rain events (Fig. 2a and Fig. S1a). However, because of very variable time lengths and intervals among different events, it is difficult to describe the common pattern of $[NH_4^+]$ variations observed in different rain events. Therefore, in order to achieve a clearer intra-event pattern of precipitation $[NH_4^+]$ variations, the time lengths (T) from sampling time points to the beginning time point of corresponding rain events were converted to Ln values (i.e., Ln [T]) (Fig. 2 and Fig. S1). The differences of $[NH_4^+]$ between adjacent sample collections (hereafter as $\Delta[NH_4^+]$) were calculated by using the $[NH_4^+]$ of the later sample minus that of the former one (Fig. 2a). Accordingly, positive, zero, and negative $\Delta[NH_4^+]$ values indicated decreases, no difference and increases of precipitation $[NH_4^+]$ across rain events. Finally, collections with similar Ln [T] values in the same stage of all events were grouped to show a common $\Delta[NH_4^+]$ pattern (Fig. 2a). The mean ± SE values of $\Delta[NH_4^+]$ values were -50.6 ± 28.3 μmol/L, -35.2 ± 18.1 μmol/L, -28.5 ± 8.7 μmol/L and -1.6 ± 5.9 μmol/L across the first stage, 16.4 ± 11.0 μmol/L across the second stage, -6.1 ± 14.3 μmol/L, -0.6 ± 15.4 μmol/L and 30.2 ± 22.2 μmol/L across the third stage (Fig. 2a).

3.2. Precipitation $\delta^{15}N$-NH_4^+ values along the time course of rain events

The $\delta^{15}N$-NH_4^+ values varied between −35.3‰ and −3.6‰ for rain samples in this work, also showing distinct intra-event fluctuations (with magnitude of 0 − 20.7‰ between adjacent sample collections) (Fig. S1b). Similar to that of $[NH_4^+]$, a decreasing pattern existed for the $\delta^{15}N$-NH_4^+ values along the time course of almost all events, but the $\delta^{15}N$-NH_4^+ variations generally exhibited three stages of decreasing, increasing, and decreasing across the rain events (Fig. 2b and Fig. S1b). The differences of $\delta^{15}N$-NH_4^+ values between adjacent sample collections (hereafter as $\Delta\delta^{15}N$-NH_4^+ values) were also calculated by using the $\delta^{15}N$-NH_4^+ values of the later sample minus that of the former one (Fig. 2b). Also, collections with similar Ln [T] values in the same stage of all events were grouped to show a common $\Delta\delta^{15}N$-NH_4^+ pattern (Fig. 2b). The mean ± SE values of $\Delta\delta^{15}N$-NH_4^+ values were $-3.4 \pm 1.6‰$, $-1.6 \pm 2.6‰$, $-2.6 \pm 1.0‰$ and $-1.5 \pm 1.2‰$ across the first stage, $2.6 \pm 0.8‰$ across the second stage, $0.4 \pm 0.7‰$, $-1.1 \pm 1.1‰$ and $-0.5 \pm 2.2‰$ across the third stage (Fig. 2b). Distinctly, both $\Delta[NH_4^+]$ and $\Delta\delta^{15}N$-NH_4^+ values showed significant increases in the fifth grouping, i.e., the second stage, before which continuous decreases were observed across the first stage. Differently, most $\Delta[NH_4^+]$ or $\Delta\delta^{15}N$-NH_4^+ values turned back to be negative in the third stage.

4. Discussion

Atmospheric NH_3 and p-NH_4^+ are direct sources of w-NH_4^+ (Kajino and Aikawa, 2015). The general decreases of precipitation $[NH_4^+]$ aross rain events (Fig. 2a and Fig. S1a) indicated more rapid removal than replenishment of NH_3 and p-NH_4^+ in the atmosphere. In other words, the concentration pattern (Fig. 2a) showed a distinct decrease of atmospheric NH_3 and p-NH_4^+ available to precipitation scavenging along the time course of rain events. However, this could not provide insights into the relative importance between NH_3 and p-NH_4^+ during precipitation scavenging processes.

Precipitation $\delta^{15}N$-NH_4^+ values may integrate $\delta^{15}N$ values of NH_3 and p-NH_4^+ sources and isotopic effects of scavenging processes (Altieri et al., 2014). The rainout and washout of NH_3 and p-NH_4^+ are major processes regulating precipitation $\delta^{15}N$-NH_4^+ values along the time course of rain events (Andronache, 2003; Dusek et al., 2006). Across a rain event, precipitation $\delta^{15}N$-NH_4^+ variations can be resulted from two main aspects: (1) physical and chemical processes related to precipitation scavenging of NH_3 and p-NH_4^+; (2) proportional contributions between NH_3 and p-NH_4^+ with different $\delta^{15}N$ values (Fig. 1).

First, the rainout and washout of p-NH_4^+ include nucleation scavenging and impaction scavenging (Andronache, 2003), during which no substantial isotope effects were assumed (Altieri et al., 2014; Liu et al., 2017). For the scavenging of NH_3 into rain drops, precipitation $\delta^{15}N$-NH_4^+ values were mainly influenced by the diffusion, ionization and equilibrium processes (Li et al., 2012; Xiao et al., 2015). The NH_3 diffusion into the rain drops has a kinetic

isotope effect, resulting in relatively ^{15}N-depleted w-NH_4^+ than NH_3 (Xiao et al., 2015). Accordingly, if NH_3 diffusion dominated intra-event precipitation δ^{15}N-NH_4^+ variations, it should have increased δ^{15}N-NH_4^+ values in rainwater along the time course of rain events because the ^{14}N-enriched NH_3 prefers to be accumulated in rain samples in earlier collections of rain events (Fry, 2006). Isotope fractionations during the ionization process ($NH_{3(aq)} \rightarrow NH_{4(aq)}^+$) has been assumed to be small or negligible (Delwiche and Steyn, 1970; Högberg, 1997). However, the $NH_{3(gas)} \leftrightarrow NH_{4(aq)}^+$ equilibrium would cause δ^{15}N fractionations of 36‰ (Moore, 1977), 31‰ (Freyer, 1978), and 29.7‰ (Hanschmann, 1981) in w-NH_4^+. Recently, isotope effects of the $NH_{3(gas)} \leftrightarrow NH_{3(aq)}$ equilibrium were also found to be high (>7.6‰; Li et al., 2012), causing relatively ^{15}N-enriched w-NH_4^+ than NH_3. In this study, precipitation δ^{15}N-NH_4^+ values (−35.3‰ to −3.6‰; Fig. S1b) were not significantly higher than those of the δ^{15}N-NH_3 values (−16.7‰; Fig. 1), suggesting that the equilibria did not dominate precipitation δ^{15}N-NH_4^+ signatures and variations (Fig. S1b). Besides, NH_3 emissions and its transportation with air mass during the rain events potentially influenced the precipitation [NH_4^+] and δ^{15}N-NH_4^+ variations (Fig. 2). The back-trajectory analyses during rain events (2 h) showed that the ranges of air mass movements were generally less than 100 km (Fig. S2), indicating a negligible influence from NH_3 emissions and p-NH_4^+ transportation from areas out of Guizhou province. According to the total amount of NH_3 emissions estimated for Guizhou province (466.8 kt in 2010; Greenhouse Gas and Air Pollution Interactions and Synergies Model; available online: http://www.iiasa.ac.at/), the proportion of NH_3 emission amount (3.6 mg-N; calculated for the sampler area) to precipitation NH_4^+ amount (c.a. 103.6 mg-N; calculated for the sampler area) during the rain events (2 h) averaged 3.5%. Accordingly, NH_3 emissions and transport should not be responsible for the observed variations of NH_4^+ concentrations and isotopes across our rain events.

Second, the intra-event δ^{15}N-NH_4^+ variations exhibited a uniform pattern that includes three-stage variations of decreasing, increasing, and decreasing along the time course of rain events (Fig. 2b), which reflected different contributions between NH_3 and p-NH_4^+. As the δ^{15}N-NH_3 values are significantly lower than δ^{15}N values of p-NH_4^+ (Fig. 1), the δ^{15}N-NH_4^+ decreases across the first stage (Fig. 2b) were primarily attributed to more decreases in scavenging p-NH_4^+ than NH_3 (Fig. 3 and Fig. S1a). Then the δ^{15}N-NH_4^+ increases across the second stage (Fig. 2b) were primarily resulted from more increases in scavenging p-NH_4^+ than NH_3 (Fig. 3 and Fig. S1a). Finally, the δ^{15}N-NH_4^+ decreases across the third stage were mainly caused by more decreases in scavenging p-NH_4^+ than NH_3 (Fig. 3 and Fig. S1a).

In order to more clearly interpret the relative importance between NH_3 and p-NH_4^+ in regulating precipitation δ^{15}N-NH_4^+ variations, the isotope mass-balance method based on the Stable Isotope Analysis in R (named SIAR model; http://cran-project.org/web/packages/siar/index.html; Parnell, and Jackson, 2008) was used to estimate the proportional contributions (F) of NH_3 and p-NH_4^+ to w-NH_4^+ (Fig. 3). The SIAR model uses the Markov Chain Monte Carlo procedure to establish a logical prior distribution for estimating F values, and then to determine the probability distribution for the F values of each source (NH_3 and NH_4^+ in $PM_{2.5}$ or TSP; Fig. 1) to the mixture (w-NH_4^+; Fig. S1b). By considering the variabilities of δ^{15}N values in both sources and precipitation, this model potentially provides reliable estimations of NH_3 and p-NH_4^+ to w-NH_4^+. In this work, due to the lack of local source data, our calculations were based on the assumption that δ^{15}N values of NH_3 and p-NH_4^+ at our study site also differ distinctly as those typical values reported throughout the globe (Fig. 1). Because $PM_{2.5}$ have been included in and mixed with the coarse particulates during the collection of TSP, $\delta^{15}N_{TSP\text{-}NH4+}$ values were used as δ^{15}N values of p-NH_4^+ in this study. On average, the NH_3 contributed 67 − 93% (relative to TSP-NH_4^+) for groupings of all three stages (Fig. 3). Across the first stage, proportional contributions of TSP-NH_4^+ decreased from 33% to 7%, while those of NH_3 increased correspondingly (Fig. 3). Because precipitation [NH_4^+] also decreased distinctly across the first stage (Fig. 2a and Fig. S1a), decreases in scavenging amounts of p-NH_4^+ were actually more than those of NH_3 (Fig. 3 and Fig. S1a). This is the main reason for decreasing precipitation δ^{15}N-NH_4^+ values across the first and third stages (Fig. 2b). Similarly, the increases of δ^{15}N-NH_4^+ values across the second stage were resulted primarily from more increases in scavenging amounts of p-NH_4^+ than those of NH_3 (Fig. 3 and Fig. S1a). Besides, $PM_{2.5}$-NH_4^+ might dominate the p-NH_4^+ scavenged by precipitation across the second and third stages. First, it has been known that during the rainout, cloud droplets scavenged $PM_{2.5}$ mostly (Heintzenberg et al., 1989; Hao et al., 2013), which would dominate in the later stages of rain events (Aikawa et al., 2014). Second, atmospheric particulates (particularly for coarse ones) are efficiently removed via washout at the beginning of rain events (Greenfield, 1957; Andronache, 2003; Aikawa et al., 2014). Accordingly, the proportional contributions between NH_3 and

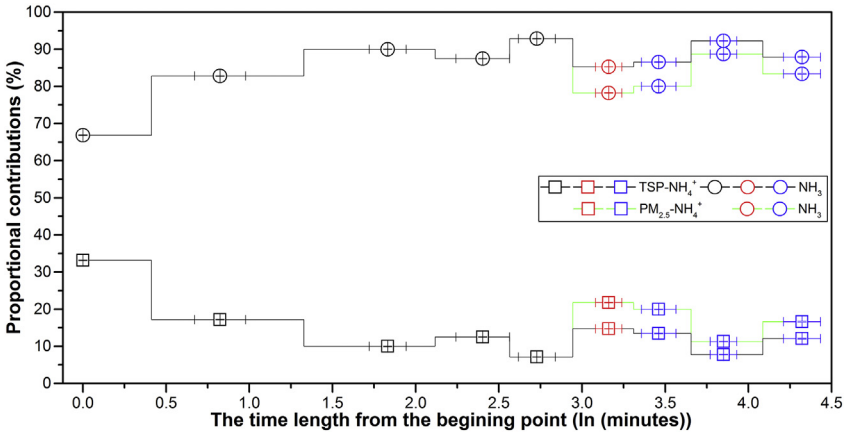

Fig. 3. Proportional contributions of NH_3 and p-NH_4^+ to w-NH_4^+ along the time course of rain events at Guiyang, SW China. Proportional contributions were estimated using δ^{15}N values of atmospheric NH_x (NH_3 and NH_4^+ in $PM_{2.5}$ or TSP; Fig. 1) and w-NH_4^+ (Fig. S1b) in the SIAR model. The percentage data ($n = 10000$) output from this model for each grouping were used for calculating the mean ± SE values. For the first stage, NH_3 and TSP-NH_4^+ were regarded as sources. For the second and third stages, analyses of two scenarios (Scenario 1: NH_3 and NH_4^+ in TSP as sources, Scenario 2: NH_3 and NH_4^+ in $PM_{2.5}$ as sources; explained in the Discussion) were conducted.

$PM_{2.5}$-NH_4^+ to w-NH_4^+ were also evaluated specifically for the second and third stages (Fig. 3).

Previously, the scavenging of particulate pollutants has been evaluated by measuring the concentrations of pollutants in particulates and precipitation that simultaneously collected, which was also performed on precipitation removal of p-NH_4^+ (Cheng and Zhang, 2017; Xu et al., 2017). However, it remains very difficult to adequately constrain the scavenging of NH_3 and coarse p-NH_4^+. From this perspective, our isotopic evidence provided a clearer understanding of how different scavenging between NH_3 and p-NH_4^+ influenced intra-event δ^{15}N-NH_4^+ variations, which is useful for better modeling precipitation scavenging of atmospheric p-NH_4^+.

5. Conclusion

Generally decreased NH_4^+ concentrations along the course of rain events investigated by Xiao et al. (2015) reflected decreasing scavenging of NH_3 and p-NH_4^+, while different scavenging between NH_3 and p-NH_4^+ was the main regulating factor for intra-event δ^{15}N-NH_4^+ variations. Using the δ^{15}N values of NH_3, $PM_{2.5}$-NH_4^+, and TSP-NH_4^+, proportional contributions of these precursors to w-NH_4^+ were further evaluated by a Bayesian isotope mixing model. The intra-event δ^{15}N-NH_4^+ decreases were primarily attributed to the more decreases in scavenging ^{15}N-enriched p-NH_4^+ than ^{15}N-depleted NH_3, while intra-event δ^{15}N-NH_4^+ increases were mainly due to more increases in scavenging p-NH_4^+, especially $PM_{2.5}$-NH_4^+, than NH_3. This study revealed useful mechanisms for using precipitation δ^{15}N-NH_4^+ values to better interpret major sources of atmospheric NH_3, as well for modeling precipitation scavenging of atmospheric p-NH_4^+.

Acknowledgements

This work was supported by the National Key Research and Development Program of China (2017YFC0210101), the National Natural Science Foundation of China (Nos. 41730855, 41522301, 41603007, 41703005), the 11th Recruitment Program of Global Experts (the Thousand Talents Plan) for Young Professionals granted by the central budget of China, and Outstanding Youth Funds of Tianjin, China. (No. 17JCJQJC45400).

Appendix A. Supplementary data

Supplementary data related to this article can be found at https://doi.org/10.1016/j.envpol.2018.04.015.

References

Aikawa, M., Hiraki, T., 2009. Washout/rainout contribution in wet deposition estimated by 0.5 mm precipitation sampling/analysis. Atmos. Environ. 43, 4935–4939.
Aikawa, M., Kajino, M., Hiraki, T., Mukai, H., 2014. The contribution of site to washout and rainout: precipitation chemistry based on sample analysis from 0.5 mm precipitation increments and numerical simulation. Atmos. Environ. 95, 165–174.
Altieri, K.E., Hastings, M.G., Peters, A.J., Oleynik, S., Sigman, D.M., 2014. Isotopic evidence for a marine ammonium source in rainwater at Bermuda. Glob. Biogeochem. Cycle. 28, 1066–1080.
Andronache, C., 2003. Estimated variability of below-cloud aerosol removal by rainfall for observed aerosol size distributions. Atmos. Chem. Phys. 3, 131–143.
Andronache, C., 2004. Estimates of sulfate aerosol wet scavenging coefficient for locations in the Eastern United States. Atmos. Environ. 38, 795–804.
Asman, W.A.H., Sutton, M.A., Schjorring, J.K., 1998. Ammonia: emission, atmospheric transport and deposition. New Phytol. 139, 27–48.
Behera, S.N., Sharma, M., Aneja, V.P., Balasubramanian, R., 2013. Ammonia in the atmosphere: a review on emission sources, atmospheric chemistry and deposition on terrestrial bodies. Environ. Sci. Pollut. Res. 20, 8092–8131.
Buda, A.R., DeWalle, D.R., 2009. Using atmospheric chemistry and storm track information to explain the variation of nitrate stable isotopes in precipitation at a site in central Pennsylvania, USA. Atmos. Environ. 43, 4453–4464.
Chang, Y.H., Liu, X.J., Deng, C.R., Dore, A.J., Zhuang, G.S., 2016. Source apportionment of atmospheric ammonia before, during, and after the 2014 APEC summit in Beijing using stable nitrogen isotope signatures. Atmos. Chem. Phys. 16, 11635–11647.
Cheng, I., Zhang, L., 2017. Long-term air concentrations, wet deposition, and scavenging ratios of inorganic ions, HNO_3 and SO_2 and assessment of aerosol and precipitation acidity at Canadian rural locations. Atmos. Chem. Phys. 17, 4711–4730.
Delwiche, C.C., Steyn, P.L., 1970. Nitrogen isotope fractionation in soils and microbial reactions. Environ. Sci. Technol. 4, 929–935.
Dusek, U., Frank, G.P., Hildebrandt, L., Curtius, J., Schneider, J., Walter, S., Chand, D., Drewnick, F., Hings, S., Jung, D., Borrmann, S., Andreae, M.O., 2006. Size matters more than chemistry for cloud-nucleating ability of aerosol particles. Science 312, 1375–1378.
Felix, J.D., Elliott, E.M., Gish, T., McConnell, L.L., Shaw, S.L., 2013. Characterizing the isotopic composition of atmospheric ammonia emission sources using passive samplers and a combined oxidation-bacterial denitrifier approach. Rapid Commun. Mass Spectrom. 27, 2239–2246.
Felix, J.D., Elliott, E.M., Gish, T., Maghirang, R., Cambal, L., Clougherty, J., 2014. Examining the transport of ammonia emissions across landscapes using nitrogen isotope ratios. Atmos. Environ. 95, 563–570.
Felix, J.D., Elliott, E.M., Avery, G.B., Kieber, R.J., Mead, R.N., Willey, J.D., Mullaugh, K.M., 2015. Isotopic composition of nitrate in sequential Hurricane Irene precipitation samples: implications for changing NO_x sources. Atmos. Environ. 106, 191–195.
Felix, J.D., Elliott, E.M., Gay, D.A., 2017. Spatial and temporal patterns of nitrogen isotopic composition of ammonia at U.S. ammonia monitoring network sites. Atmos. Environ. 150, 434–442.
Freyer, H.D., 1978. Seasonal trends of NH_4^+ and NO_3^- nitrogen isotope composition in rain collected at Jülich. Ger. Tellus A30, 83–92.
Fry, B., 2006. Stable Isotope Ecology. Springer Berlin.
Galloway, J.N., Townsend, A.R., Erisman, J.W., Bekunda, M., Cai, Z.C., Freney, J.R., Martinelli, L.A., Seitzinger, S.P., Sutton, M.A., 2008. Transformation of the nitrogen cycle: recent trends, questions, and potential solutions. Science 320, 889–892.
Garten, C.T., 1992. Nitrogen isotope composition of ammonium and nitrate in bulk precipitation and forest throughfall. Int. J. Environ. Anal. Chem. 47, 33–45.
Georgii, H.W., Muller, W.J., 1973. On the distribution of ammonia in the middle and lower troposphere. Tellus A26, 180–184.
Greenfield, S.M., 1957. Rain scavenging of radioactive particulate matter from the atmosphere. J. Meteorol. 14, 115–125.
Guo, S., Hu, M., Zamora, M.L., Peng, J.F., Shang, D.J., Zheng, J., Du, Z.F., Wu, Z.J., Shao, M., Zeng, L.M., Molina, M.J., Zhang, R.Y., 2014. Elucidating severe urban haze formation in China. Proc. Nat. Acad. Sci. U. S. A. 111, 17373–17378.
Hanschmann, G., 1981. Berechnung von Isotopieeffekten auf quantenchemischer Grundlage am Beispiel stickstoffhaltiger Molekule. ZFI-Mitt 41, 19–39.
Hao, L.Q., Romakkaniemi, S., Kortelainen, A., Jaatinen, A., Portin, H., Miettinen, P., Komppula, M., Leskinen, A., Virtanen, A., Smith, J.N., Sueper, D., Worsnop, D.R., Lehtinen, K.E.J., Laaksonen, A., 2013. Aerosol chemical composition in cloud events by high resolution time-of-flight aerosol mass spectrometry. Environ. Sci. Technol. 47, 2645–2653.
Heaton, T.H.E., 1987. ^{15}N/^{14}N ratios of nitrate and ammonium in rain at Pretoria, South Africa. Atmos. Environ. 21, 843–852.
Heaton, T.H.E., Spiro, B., Madeline, S., Robertson, C., 1997. Potential canopy influences on the isotopic composition of nitrogen and sulphur in atmospheric deposition. Oecologia 109, 600–607.
Heintzenberg, J., Ogren, J.A., Noone, K.J., Gärdneus, L., 1989. The size distribution of submicrometer particles within and about stratocumulus cloud droplets on Mt. Åreskutan, Sweden. Atmos. Res. 24, 89–101.
Hoering, T., 1956. The isotopic composition of the ammonia and the nitrate ion in rain. Geochim. Cosmochim. Acta 12, 97–102.
Högberg, P., 1997. ^{15}N natural abundance in soil-plant systems. New Phytol. 137, 179–203.
Huang, X., Song, Y., Li, M.M., Li, J.F., Huo, Q., Cai, X.H., Zhu, T., Hu, M., Zhang, H.S., 2012. A high-resolution ammonia emission inventory in China. Glob. Biogeochem. Cycle. 26. GB1030.
Kajino, M., Aikawa, M., 2015. A model validation study of the washout/rainout contribution of sulfate and nitrate in wet deposition compared with precipitation chemistry data in Japan. Atmos. Environ. 117, 124–134.
Kang, Y.N., Liu, M.X., Song, Y., Huang, X., Yao, H., Cai, X.H., Zhang, H.S., Kang, L., Liu, X.J., Yan, X.Y., He, H., Zhang, Q., Shao, M., Zhu, T., 2016. High-resolution ammonia emissions inventories in China from 1980 to 2012. Atmos. Chem. Phys. 16, 2043–2058.
Köhler, H., 1936. The nucleus in and the growth of hygroscopic droplets. Trans. Faraday Soc. 32, 1152–1161.
Kundu, S., Kawamura, K., Lee, M., 2010. Seasonal variation of the concentrations of nitrogenous species and their nitrogen isotopic ratios in aerosols at Gosan, Jeju Island: implications for atmospheric processing and source changes of aerosols. J. Geophys. Res. Atmos. 115. D20305.
Leng, Q.M., Cui, J., Zhou, F.W., Du, K., Zhang, L.Y., Fu, C., Liu, Y., Wang, H.B., Shi, G.M., Gao, M., Yang, F.M., He, D.Y., 2017. Wet-only deposition of atmospheric inorganic nitrogen and associated isotopic characteristics in a typical mountain area, southwestern China. Sci. Total. Environ. 616–617, 55–63.
Li, L., Lollar, B.S., Li, H., Wortmann, U.G., Lacrampe-Couloume, G., 2012. Ammonium

stability and nitrogen isotope fractionations for NH_4^+–$NH_{3(aq)}$–$NH_{3(gas)}$ systems at 20–70 °C and pH of 2–13: applications to habitability and nitrogen cycling in low-temperature hydrothermal systems. Geochim. Cosmochim. Acta 84, 280–296.

Li, L., Yin, Y., Kong, S.F., Wen, B., Chen, K., Yuan, L., Li, Q., 2014. Altitudinal effect to the size distribution of water soluble inorganic ions in PM at Huangshan, China. Atmos. Environ. 98, 242–252.

Li, J.X., Yin, Y., Li, P.R., Li, Z.Q., Li, R.J., Cribb, M., Dong, Z.P., Zhang, F., Li, J., Ren, G., Jin, L.J., Li, Y.Y., 2015. Aircraft measurements of the vertical distribution and activation property of aerosol particles over the Loess Plateau in China. Atmos. Res. 155, 73–86.

Lin, C.T., Jickells, T.D., Baker, A.R., Marca, A., Johnson, M.T., 2016. Aerosol isotopic ammonium signatures over the remote Atlantic Ocean. Atmos. Environ. 133, 165–169.

Liu, X.J., Zhang, Y., Han, W.X., Tang, A.H., Shen, J.L., Cui, Z.L., Vitousek, P., Erisman, J.W., Goulding, K., Christie, P., Fangmeier, A., Zhang, F.S., 2013. Enhanced nitrogen deposition over China. Nature 494, 459–462.

Liu, D.W., Fang, Y.T., Tu, Y., Pan, Y.P., 2014. Chemical method for nitrogen isotopic analysis of ammonium at natural abundance. Anal. Chem. 86, 3787–3792.

Liu, X.Y., Xiao, H.W., Xiao, H.Y., Song, W., Sun, X.C., Zheng, X.D., Liu, C.Q., Koba, K., 2017. Stable isotope analyses of precipitation nitrogen sources in Guiyang, southwestern China. Environ. Pollut. 230, 486–494.

Moore, H., 1977. The isotopic composition of ammonia, nitrogen dioxide and nitrate in the atmosphere. Atmos. Environ. 11, 1239–1243.

Okita, T., Hara, H., Fukuzaki, N., 1996. Measurements of atmospheric SO_2 and SO_4^{2-}, and determination of the wet scavenging coefficient of sulfate aerosols for the winter monsoon season over the Sea of Japan. Atmos. Environ. 30, 3733–3739.

Park, Y.M., Park, K.S., Kim, H., Yu, S.M., Noh, S., Kim, M.S., Kim, J.Y., Ahn, J.Y., Lee, M.D., Seok, K.S., Kim, Y.H., 2017. Characterizing isotopic compositions of TC-C, NO_3^--N, and NH_4^+-N in $PM_{2.5}$ in South Korea: impact of China's winter heating. Environ. Pollut. 233, 735–744.

Parnell, A.C., Jackson, A.L., 2008. SIAR: Stable Isotope Analysis in R. Available from: http://cran.r-project.org/web/packages/siar/index.html. (Accessed 10 December 2008).

Proemse, B.C., Mayer, B., Chow, J.C., Watson, J.G., 2012. Isotopic characterization of nitrate, ammonium and sulfate in stack $PM_{2.5}$ emissions in the Athabasca Oil Sands Region, Alberta, Canada. Atmos. Environ. 60, 555–563.

Sander, R., 2015. Compilation of Henry's law constants (version 4.0) for water as solvent. Atmos. Chem. Phys. 15, 4399–4981.

Savard, M.M., Cole, A., Smirnoff, A., Vet, R., 2017. $\delta^{15}N$ values of atmospheric N species simultaneously collected using sector-based samplers distant from sources – isotopic inheritance and fractionation. Atmos. Environ. 162, 11–22.

Sebilo, M., Mayer, B., Grably, M., Billiou, D., Mariott, A., 2004. The use of the 'ammonium diffusion' method for $\delta^{15}N$-NH_4^+ and $\delta^{15}N$-NO_3^- measurements: comparison with other techniques. Environ. Chem. 1, 99–103.

Seinfeld, J.H., Pandis, S.N., 2006. Atmospheric Chemistry Physics: from Air Pollution to Climate Change. Wiley, New York.

Skinner, R., Ineson, P., Hicks, W.K., Jones, H.E., Sleep, D., Leith, I.D., Sheppard, L.J., 2004. Correlating the spatial distribution of atmospheric ammonia with $\delta^{15}N$ values at an ammonia release site. Water Air Soil Pollut. 4, 219–228.

Skinner, R.A., Ineson, P., Jones, H., Sleep, D., Rank, R., 2006. Using $\delta^{15}N$ values to characterise the nitrogen nutrient pathways from intensive animal units. Rapid Commun. Mass Spectrom. 20, 2858–2864.

Smirnoff, A., Savard, M.M., Vet, R., Simard, M.C., 2012. Nitrogen and triple oxygen isotopes in near-road air samples using chemical conversion and thermal decomposition. Rapid Commun. Mass Spectrom. 26, 2791–2804.

Sun, Y.L., Du, W., Wang, Q.Q., Zhang, Q., Chen, C., Chen, Y., Chen, Z.Y., Fu, P.Q., Wang, Z.F., Gao, Z.Q., Worsnop, D.R., 2015. Real-time characterization of aerosol particle composition above the urban canopy in Beijing: insights into the Interactions between the atmospheric boundary layer and aerosol chemistry. Environ. Sci. Technol. 49, 11340–11347.

Sutton, M.A., Dragosits, U., Tang, Y.S., Fowler, D., 2000. Ammonia emissions from non-agricultural sources in the UK. Atmos. Environ. 34, 855–869.

Wang, S.X., Xing, J., Jang, C., Zhu, Y., Fu, J.S., Hao, J.M., 2011. Impact assessment of ammonia emissions on inorganic aerosols in east China using response surface modeling technique. Environ. Sci. Technol. 45, 9293–9300.

Wang, Y., Zhang, Q.Q., He, K., Zhang, Q., Chai, L., 2013. Sulfate-nitrate-ammonium aerosols over China: response to 2000-2015 emission changes of sulfur dioxide, nitrogen oxides, and ammonia. Atmos. Chem. Phys. 13, 2635–2652.

Wang, X., Zhang, L., Moran, M.D., 2014. Development of a new semi-empirical parameterization for below-cloud scavenging of size-resolved aerosol particles by both rain and snow. Geosci. Model. Dev. 7, 799–819.

Xiao, H.W., Xiao, H.Y., Long, A.M., Liu, C.Q., 2015. $\delta^{15}N$–NH_4^+ variations of rainwater: application of the Rayleigh model. Atmos. Res. 157, 49–55.

Xu, W., Luo, X.S., Pan, Y.P., Zhang, L., Tang, A.H., Shen, J.L., Zhang, Y., Li, K.H., Wu, Q.H., Yang, D.W., Zhang, Y.Y., Xue, J., Li, W.Q., Li, Q.Q., Tang, L., Lu, S.H., Liang, T., Tong, Y.A., Liu, P., Zhang, Q., Xiong, Z.Q., Shi, X.J., Wu, L.H., Shi, W.Q., Tian, K., Zhong, X.H., Shi, K., Tang, Q.Y., Zhang, L.J., Huang, J.L., He, C.E., Kuang, F.H., Zhu, B., Liu, H., Jin, X., Xin, Y.J., Shi, X.K., Du, E.Z., Dore, A.J., Tang, S., Collett Jr., J.L., Goulding, K., Sun, Y.X., Ren, J., Zhang, F.S., Liu, X.J., 2015. Quantifying atmospheric nitrogen deposition through a nationwide monitoring network across China. Atmos. Chem. Phys. 15, 12345–12360.

Xu, D.H., Ge, B.Z., Wang, Z.F., Sun, Y.L., Chen, Y., Ji, D.S., Yang, T., Ma, Z.Q., Cheng, N.L., Hao, J.Q., Yao, X.F., 2017. Below-cloud wet scavenging of soluble inorganic ions by rain in Beijing during the summer of 2014. Environ. Pollut. 230, 963–973.

Yamagata, S., Kobayashi, D., Ohta, S., Murao, N., Shiobara, M., Wada, M., Yabuki, M., Konishi, H., Yamanouchi, T., 2009. Properties of aerosols and their wet deposition in the arctic spring during ASTAR2004 at Ny-Alesund, Svalbard. Atmos. Chem. Phys. 9 (1), 261–270.

Yeatman, S.G., Spokes, L.J., Dennis, P.F., Jickells, T.D., 2001. Comparisons of aerosol nitrogen isotopic composition at two polluted coastal sites. Atmos. Environ. 35, 1307–1320.

Zhang, Q., Ma, X.C., Tie, X.X., Huang, M.Y., Zhao, C.S., 2009. Vertical distributions of aerosols under different weather conditions: analysis of in-situ aircraft measurements in Beijing, China. Atmos. Environ. 43, 5526–5535.

Zhang, L., Wang, X., Moran, M.D., Feng, J., 2013. Review and uncertainty assessment of size-resolved scavenging coefficient formulations for below-cloud snow scavenging of atmospheric aerosols. Atmos. Chem. Phys. 13, 10005–10025.